PCCP

Accepted Manuscript




ROYAL SOCIETY OF CHEMISTRY

www.rsc.org/pccp

Journal Name

RSCPublishing

ARTICLE

# Vibrational control of electron transfer reactions: A feasibility study for the fast coherent transfer regime

Cite this: DOI: 10.1039/xoxxoooooox

P. Antoniou,[a] Z. Ma,[b] P. Zhang,[b] D.N Beratan,[b,c,d] and S.S. Skourtis.[a,e]

Received 30th January 2012,
Accepted 00th January 2012

DOI: 10.1039/xoxxoooooox

www.rsc.org/

Molecular vibrations and electron-vibrational interactions are central to the control of biomolecular electron and energy transfer rates. The vibrational control of molecular electron transfer reactions by infrared pulses may enable precise probes of electronic-vibrational interactions and of their roles in determining electron transfer mechanisms. This type of electron-transfer rate control is advantageous because it does not alter the electronic state of the molecular electron transfer system or irreversibly change its molecular structure. For bridge-mediated electron transfer reactions, infrared (vibrational) excitation of the bridge linking the electron donor to the electron acceptor was suggested as being capable of influencing the electron transfer rate by modulating the bridge-mediated donor-to-acceptor electronic coupling. This kind of electron transfer experiment has been realized, demonstrating for the first time that bridge-mediated electron-transfer rates can be changed by exciting vibrational modes of the bridge. Here, we use simple models and ab initio computations to explore the physical constraints on one's ability to vibrationally perturb electron transfer rates using infrared excitation. These constraints stem from the nature of molecular vibrational spectra, the strengths of the electron-vibrational coupling, and the interaction between molecular vibrations and infrared radiation. With these constraints in mind, we suggest parameter regimes and molecular architectures that may enhance the vibrational control of electron transfer for fast coherent electron-transfer reactions.

## 1. Introduction

Biomolecular electron transfer and energy transfer reactions are central to bioenergetics and to cellular function [1-13]. Molecular motions are critical in determining the electron-transfer rates for long-distance biological electron-transfer reactions mediated by through-bridge tunneling. Such biomolecular ET systems have weak bridge-mediated electron-donor to electron-acceptor couplings (tunneling matrix elements), and their ET rates are nonadiabatic and relatively slow (time scales longer than ns). Low frequency molecular motions determine these nonadiabatic ET rates by modulating the donor-acceptor electronic energy gap and the donor-acceptor coupling.

More recently it was recognized that biomolecular electron and energy transfer reactions in the nearly-adiabatic or adiabatic regimes may also depend critically on bridge molecular motions that cause fluctuations in electronic site-energies and inter-site electronic couplings, or that serve as electronic energy sinks (e.g., [14-16] and references therein). In such transport systems, fast and partially coherent transport is possible over relatively large distances (greater than nm), often with high transport efficiency [16,17]. A question that is of central interest in this strong coupling regime is how molecular motion tunes the transport mechanism and how the motion influences electronic coherences (e.g., [15,16,18]). Recently, two-dimensional spectroscopy experiments provided evidence that vibrational (in addition to electronic) coherences may improve the efficiency of the primary charge separation events in photosynthesis ([19,20] and references therein). A natural approach to probing the vibrational control of electron transfer and energy transfer rates experimentally is to identify vibrational modes that influence the transport rate and to perturb these modes selectively by IR-excitation [10,21-25]. Since these biomolecular transport systems often have complex electronic and vibrational spectra, it is easier (and also useful for understanding mechanisms) to use simpler and smaller molecular model systems in both experiment and theory. Further small molecules may be used as building blocks for transport devices whose transport rates and yields may be controlled by IR excitation.

Consider a donor(D)-bridge(B)-acceptor(A) molecule that undergoes photoinduced nonadiabatic electron transfer (ET) mediated by the intervening bridge electronic states. [7-12]. Exciting the B vibrational modes before or after the electronic excitation could make it possible to control the D-A ET rate by modulating the B state energies and D-B (A-B) electronic couplings [21-24]. This idea was initially discussed in the context of molecular architectures that offer parallel D-B-A tunneling pathways [21-23]. In systems where the bridge connecting D to A provides two different electron tunneling pathways, (i.e. involving different groups of atoms), the selective excitation of B vibrational modes localized in one pathway may lead to the exchange of the excess vibrational energy of the B modes with the tunneling electron. This energy exchange leaves an inelastic-tunneling marker of the tunneling route taken by the electron and thus "labels" the path of the electron. As such, one can

built a molecular double slit experiment or a which-way interferometer based upon molecular ET [21-24].

Several challenges are faced in accomplishing the vibrational control of electron tunneling pathway interferences, as the interferences are sensitive to thermal structural fluctuation and to dephasing [10,23,26]. A more modest goal is to perturb the D-B-A ET rate by modulating the elastic bridge-mediated D-A tunneling interaction [9,10]. The first experiment that performed this modulation was reported in ref [25] using mid-IR pulses with UV-pump/mid-IR/vis-probe spectroscopy. The ET system has an anthracene-derived acceptor connected to a dimethylaniline-containing donor linked by guanosine-cytidine (GC) hydrogen bonds. Mid-IR excitation was targeted to drive bridge G-C H-bond motion that influences the D-A coupling. The reported fractional changes in charge separation and recombination rates were a few percent. More recently, ET rate modulation by IR excitation was demonstrated in ref [27] for an electronically excited covalent trans-acetylide platinum(II) D-B-A system. Excitation of the high frequency bridge triple carbon-carbon bond vibrations leads to the switching off ET. In addition, Ref [28] reported IR-induced ET rate modulations of 28% in Re(I) D-A complexes. In spite of the theoretical [21-24] and recent experimental progress [27-34], it remains challenging to explain the rate modulation in these systems and to design new systems that enable enhanced control of ET rate by IR excitation.

ET rate control is an example of quantum transport driven by external fields [35,36]. The aims of this study are to further explore the feasibility of perturbing bridge-mediated ET rates by exciting selected B vibrations with infrared (IR) pulses and to suggest simple experimental observables and molecular architectures to enable the measurement of IR-induced ET rate perturbations. The advantage of using B vibrations (rather than D or A vibrations) to perturb bridge-mediated ET rates is derived from the possibility of manipulating ET pathways – and thus kinetics - selectively, without interfering with the initial (D) and final (A) electronic states of the reaction.

## 2. Results and discussion

What experimental observables can be used to probe the effects of IR excitation on the ET rate? What are that donor-bridge-acceptor (DBA) rate-network architectures that enable effective control of ET rates by IR excitation? Below we first discuss simple examples using simple kinetic (rate) models that suggest answers to these questions.

### 2.1 Observables and architectures

We consider first a linear DBA system and an experiment where a UV (VIS) pulse excites the D electronic state to initiate ET, and an IR pulse excites the selected B vibrational modes (Fig. 1). The final D and/or A state population is probed directly by UV (VIS) pulses (pump-probe experiment). We assume for simplicity that the D-to-A ET rate is much faster than the back rate (both with and without the IR pulse), and we ignore the backward rate (this assumption does not change the final generic conclusions, but it gives simple analytical expressions). In the absence of the IR pulse, the ET rate is $k$. The IR pulse changes $k$ for a period of time (related to the width of the pulse and to the time scale of vibrational relaxation), i.e. $k \to k(t)$. The changes in this rate may be derived from quantum interference effect linked to the IR-pulse, to changes in the conformational energy landscape, or to other sources. In the absence of IR excitation, the rate equations are $dP_D(t)/dt = -kP_D(t)$ and $dP_A(t)/dt = kP_D(t)$, and the A state population is given by $P_A(t) = P_D(0)\left[1-\exp(-kt)\right]$ with $P_A(\infty) = P_D(0)$. With IR excitation, the rate is changed $k \to k(t)$, and the final A state population is given by $P_A(t) = P_D(0)\left\{1-\exp\left(-\int_0^t dt' k(t')\right)\right\}$ with $P_A(\infty) = P_D(0)$. Thus, the pulse does not change the final A population. The population changes induced by IR excitation are transient and disappear some time after the application of the pulse.

Fig. 2 shows an example where the D electronic state participates in an irreversible chemical reaction that produces the product X, i.e., $dP_X(t)/dt = k_{D\to X}P_D(t)$. The infinite time yield of the product X is $Y_X(\infty) = k_{D\to X}\int_0^\infty dt\, P_D(t)$. We assume that $k_{D\to X} \ll k$ so that the time evolution of the D population is determined predominantly by ET to A. An IR pulse impinging on the bridge at time $t_0$ produces a time dependent ET rate perturbation, i.e., $k^{(IR)} = k + \delta k^{(IR)}(t)$, where $\delta k^{(IR)}(t) = \delta k^{(IR)} \times f(t-t_0)$ and $f(t-t_0)$ is a normalized function with width $\sigma_t$. $\delta k^{(IR)}$ will be shown generally to be a small perturbation (assuming that the influence of the IR excitation on the molecule is nondestructive and reversible). For $t >> t_0 + \sigma_t$, the D survival probability is $P_D^{(IR)}(t) \approx P_D(0)\exp\left(-\left(k+\delta k^{(IR)}\right)t\right)$. The fractional change in the $D \to X$ reaction yield upon application of the IR pulse is

$$I = \frac{Y_X^{(IR)}(\infty) - Y_X(\infty)}{Y_X(\infty)} = \frac{\int_0^\infty dt\left(P_D^{(IR)}(t) - P_D(t)\right)}{\int_0^\infty dt P_D(t)} \approx -\frac{\delta k^{(IR)}}{\left(k+\delta k^{(IR)}\right)} \approx -\frac{\delta k^{(IR)}}{k} \quad (1)$$

Therefore, we can measure time-dependent changes in the ET rates induced by application of an IR pulse by measuring the yield of a competing reaction from the photochemically prepared D state.

The above examples considered a linear DBA architecture. For more complex architectures (and rate network connectivities), perturbations of the ET rates by finite IR pulses change both the long-time populations and yields. For example, consider a donor D connected to left and right B units ($B_L$, $B_R$), each with independent A moieties ($A_L$, $A_R$), (Fig. 3). Photoinduced ET may proceed to $A_L$ and to $A_R$ with rates $k_L$ and $k_R$, respectively. The rate equations are $dP_D(t)/dt = -(k_L+k_R)P_D(t)$, $dP_{A_L}(t)/dt = k_L P_D(t)$ and $dP_{A_R}(t)/dt = k_R P_D(t)$. Therefore,



 

$$\frac{P_{A_L}(\infty)}{P_{A_R}(\infty)} = \frac{k_L}{k_R} \quad (2a)$$

$$\frac{P_{A_L}(\infty) - P_{A_R}(\infty)}{P_{A_L}(\infty) + P_{A_R}(\infty)} = \frac{k_L - k_R}{k_L + k_R} \quad (2b)$$

For a symmetric system with $k_L = k_R = k$, (e.g. $B_L = B_R$ and $A_L = A_R$), selective excitation of IR vibrational modes on one of the B units, (e.g., $B_L$) may be accessible if isotopic substitutions are made to one of the units [21-23]. If D is prepared in its electronic excited state and $B_L$ is excited by the IR pulse, then $k_L = k + \delta k^{(IR)}(t)$. The ratios in eqn (2) become

$$\frac{P_{A_L}(\infty)}{P_{A_R}(\infty)} \approx \frac{k + \delta k^{(IR)}}{k} \quad (3a)$$

$$\frac{P_{A_L}(\infty) - P_{A_R}(\infty)}{P_{A_L}(\infty) + P_{A_R}(\infty)} \approx \frac{\delta k^{(IR)}}{2k} \quad (3b)$$

(assuming a weak perturbation $\delta k^{(IR)}(t) = \delta k^{(IR)} \times f(t - t_0)$). The asymmetry in the L/R A populations following the IR pulse (eqn (3b)) is a direct measure of $\delta k^{(IR)}$. Further, if $A_L$ and $A_R$ participate in separate reactions that produce the products $X_L$ and $X_R$ i.e., $dP_{X_{L(R)}}(t)/dt = k_{A_{L(R)} \to X_{L(R)}} P_{A_{L(R)}}(t)$, then

$$\frac{Y_{A_L}(\infty)}{Y_{A_R}(\infty)} \approx \frac{k + \delta k^{(IR)}}{k} \quad , \quad (4a)$$

and

$$\frac{Y_{A_L}(\infty) - Y_{A_R}(\infty)}{Y_{A_L}(\infty) + Y_{A_R}(\infty)} \approx \frac{\delta k^{(IR)}}{2k} \, , \quad (4b)$$

(assuming $k_{A_L \to X_L} \approx k_{A_R \to X_R} \ll k$).

In summary, the influence of time-dependent IR perturbations on ET rates can be measured using time-independent observables (e.g., long-time populations and reaction yields) if secondary reactions compete with ET. ET systems with a single D and multiple A units (connected by independent links) are good candidates for directly measuring the influence of IR pulses on ET rates. Importantly, in such systems, pulsed-IR excitation can change the relative populations and yields of the charge-separated states, and may influence the directionality of ET without causing irreversible photochemical changes to the ET structures. The ability to change the yields of competing reactions using small external fields is familiar in the context of magnetic sensing by molecular and biomolecular compasses, where a weak external magnetic field affects the yield ratio of singlet and triplet reaction products produced by ET [37].

### 2.2 The IR perturbation of ET rates: low- vs high-frequency ET-active vibrations

Next, we switch to a quantum mechanical (rather than kinetic model) formulation to examine molecular bridge (B) vibrations that can perturb ET rates through their excitation. Given a candidate DBA molecule for vibrational control of the ET rate, the first step is to identify the B vibrations that influence ET by modulating the B electronic state energies and/or D-B (A-B) electronic couplings. These "ET-active" modes may be of low and/or high frequency. Since vibrational energy relaxation time scales are usually in the range of hundreds fsec to a few psec [38-40], there are different strategies to perturb bridge-mediated ET by IR excitation of bridge modes. These strategies depend on the time scale of ET and on the nature of the ET-active modes. The typical vibrational-relaxation and energy-redistribution times of excited vibrational modes in molecules are sub-ps to a few ps for high-frequency modes. We first consider the case of high-frequency IR-active / ET-active bridge vibrational modes ($\hbar\omega >> K_B T$). Modes of this kind are targets for IR control of ET because they can be selectively excited and they remain in an excited state for a relatively long time, as they are not embedded in a mode continuum that produces rapid IVR. If the ET timescale is of the order of the mode lifetime, then an experiment with ET initiation followed by IR excitation of the high-frequency ET-active modes (Fig. 1) could modulate the ET rate "as the electron transfers" and possibly while the transfer is still coherent.

### 2.3 The Modulating ET by IR excitation of a high-frequency ET-active vibration

In previous studies [21-24], we introduced the idea of IR-modulation of ET in the context of simple quantum mechanical Hamiltonian models. Here we switch to a density matrix formulation that takes into account the effects of vibrational relaxation. These effects are critical since the de-excitation of the IR-vibrations that are selected for ET rate modulation will influence the magnitude of modulation. Further, in this study we aim to explore realistic ET system and experimental parameter regimes that are likely to be optimal for the IR perturbation of ET rates and yields (e.g., electronic structure parameters, vibrational and electron-phonon coupling parameters, IR-molecule coupling parameters and IR-pulse characteristics).

Our simple model D-B-A ET system (Fig. 1) incorporates vibrational relaxation and IR perturbation. The DBA system (S) Hamiltonian is

$$\hat{H}_S = \hat{H}_D + \hat{H}_B + \hat{H}_A + \hat{V}_{DB} + \hat{V}_{AB} \, , \quad (5)$$

where $\hat{H}_D$, $\hat{H}_B$ and $\hat{H}_A$ are vibronic D, B and A Hamiltonians; $\hat{V}_{DB}$ and $\hat{V}_{AB}$ are D-B and A-B electronic interaction Hamiltonians. Each of the D, B and A Hamiltonians are of the form

$$\hat{H}_K = \hat{H}_K^{el} + \hat{H}_K^{vi} + \hat{H}_K^{el-vi} \quad (K = D, B, A), \quad (6)$$

where "el" denotes electronic, "vi" vibrational and "el-vi" electronic-vibrational-coupling. $\hat{H}_K^{el}$ describe site energies for the relaxed D, B and A electron (or hole) states (the energies are denoted $E_D^0$, $E_B^0$ and $E_A^0$, respectively). $\hat{H}_K^{vi}$ describe the high-frequency modes that

are perturbed by ET and that may also be excited by IR. For $\hat{H}_K^{el-vi}$, we assume linear electron-vibrational coupling. The $\hat{V}_{DB}$ and $\hat{V}_{AB}$ Hamiltonians contain the D-B and A-B electronic couplings. We consider a system that is coupled to two high-frequency vibrational modes. The first oscillator (frequency $\omega_B$) is perturbed when the electron occupies the B state and the second oscillator (frequency $\omega_A$) is perturbed when the electron occupies the A state (Fig. 4a). For each of the oscillators, we denote the oscillator eigenstates in the absence of the electron-vibrational coupling as "unrelaxed" and use the symbol $|n^u\rangle$. With the electron-vibrational coupling turned on, we denote the oscillator eigenstates as "relaxed" and we use the symbol $|n^R\rangle$. In summary, the system electronic Hamiltonian is

$$\hat{H}^{el} = E_D^0 |D\rangle\langle D| + E_B^0 |B\rangle\langle B| + E_A^0 |A\rangle\langle A| + V_{DB}^{el}\left(|D\rangle\langle B| + |B\rangle\langle D|\right) + V_{AB}^{el}\left(|B\rangle\langle A| + |A\rangle\langle B|\right). \quad (7)$$

In the unrelaxed oscillator representation, the vibrational Hamiltonian is

$$\hat{H}^{vi} = \sum_{n_B^u} \hbar\omega_B \left(n_B^u + \frac{1}{2}\right) |n_B^u\rangle\langle n_B^u| + \sum_{n_A^u} \hbar\omega_A \left(n_A^u + \frac{1}{2}\right) |n_A^u\rangle\langle n_A^u| \quad (8)$$

and the electron-vibrational interaction Hamiltonian is

$$\hat{H}^{el-vi} = \left(|B\rangle\langle B|\right) \otimes \left[-\Delta F_B \hat{R}\right] + \left(|A\rangle\langle A|\right) \otimes \left[-\Delta F_A \hat{R}'\right] \quad (9)$$

where $\hat{R}$ and $\hat{R}'$ are the displacements of the B and A oscillators and $\Delta F_B$, $\Delta F_A$ are the forces exerted by the electron on the B and A oscillators. The vibronic states of the system are product states. For example, in the unrelaxed representation, $|el; vi, vi'\rangle = |el\rangle |n_B^u\rangle |n_A^u\rangle$, where $el = D$, $B$ or $A$. Using dimensionless displacements for the oscillators in eqn (9), i.e. $\hat{s} = \hat{R}/\sqrt{\hbar/2m_B\omega_B}$, $\hat{s}' = \hat{R}'/\sqrt{\hbar/2m_A\omega_A}$, the electron-vibrational coupling terms are $\left(|B\rangle\langle B|\right) \otimes a_B \hat{s}$ and $\left(|A\rangle\langle A|\right) \otimes a_A \hat{s}'$, where $a_B = -\Delta F_B \sqrt{\hbar/2m_B\omega_B}$ and $a_A = -\Delta F_A \sqrt{\hbar/2m_A\omega_A}$ are in units of energy (Fig. 4b).

The interaction of the B oscillator with the IR field is described by the Hamiltonian:

$$\hat{V}_{B,IR}(t) = -\frac{\partial \hat{\mu}_{B,IR}}{\partial R} \hat{R}\, E(t-\tau, \Omega_{IR}, \sigma_{IR}) = -\frac{\partial \hat{\mu}_{B,IR}}{\partial R} \hat{R}\, E_0\, e^{-(t-\tau)^2/2\sigma_{IR}^2} \cos\left(\Omega_{IR} t\right) \quad (10)$$

where $E_0$ is the field intensity. $\hat{\mu}_{B,IR}$ is the vibronic dipole operator, and $E(t-\tau, \Omega_{IR}, \sigma_{IR})$ represents a Gaussian electric field pulse of frequency $\Omega_{IR}$ centered at time $\tau$ with width $\sigma_{IR}$. The IR frequency is assumed to be resonant with a vibrational transition of the B oscillator. Setting $\hat{s} = \hat{R}/\sqrt{\hbar/2m\omega}$ gives $\hat{V}_{B,IR}(t) = -a_{IR}\, e^{-(t-\tau)^2/2\sigma_{IR}^2} \cos\left(\Omega_{IR} t\right)$, where the IR field-to-mode coupling strength is $a_{IR} = E_0 \left(\partial\mu_{B,IR}/\partial R\right)\sqrt{\left(\hbar/2m_B\omega_B\right)}$ (in units of energy).

The effect of vibrational energy transfer and relaxation of the two oscillators, due to interactions with the remaining vibrational degrees of freedom, are included in the dissipative relaxation terms. The time evolution of vibronic populations and coherences of the system is described by a stochastic Liouville equation for the system density matrix $\hat{\sigma}(t)$, given by:

$$i\hbar \frac{d\hat{\sigma}(t)}{dt} = \hat{L}^{coh}(t)\hat{\sigma}(t) + \hat{L}^{diss}\hat{\sigma}(t) \quad (11)$$

where $\hat{L}^{coh}(t)\hat{\sigma}(t) = \left[\hat{H}_S + \hat{V}_{B,IR}(t), \hat{\sigma}(t)\right]$ is the coherent part and $\hat{L}^{diss}\hat{\sigma}(t)$ is the dissipative part, chosen to have the Lindbland form that preserves the total probability. The dissipative part contains decay rates $\Gamma_{\nu\to\nu'}^{rel}$ between vibrational states $\nu$ and $\nu'$ of the system modes, i.e:

$$\hat{L}^{rel}\hat{\sigma} = i\hbar \sum_{\nu,\nu'} \hat{R}_{\nu\to\nu'}^{rel} \hat{\sigma} \hat{R}_{\nu\to\nu'}^{rel\,\dagger} - \frac{1}{2}\left(\hat{R}_{\nu\to\nu'}^{rel\,\dagger} \hat{R}_{\nu\to\nu'}^{rel} \hat{\sigma} + \hat{\sigma} \hat{R}_{\nu\to\nu'}^{rel\,\dagger} \hat{R}_{\nu\to\nu'}^{rel}\right) \quad (12)$$

where $\hat{R}_{\nu\to\nu'}^{rel} = \sqrt{\Gamma_{\nu\to\nu'}^{rel}}\, |\nu'\rangle\langle\nu|$ (Fig. 4b). In the basis of vibronic states in the unrelaxed representation, eqn (11) and (12) become

$$i\hbar \frac{\partial \sigma_{el;n_i,n_i';el';n_j,n_j'}(t)}{\partial t} = \left[\hat{H}_S + \hat{V}_{B,IR}(t), \hat{\sigma}(t)\right]_{el;n_i,n_i';el';n_j,n_j'} + i\hbar\Gamma_B^{rel} \left[\begin{array}{l} \sqrt{n_i+1}\sqrt{n_j+1}\langle el; n_i+1, n_i' | \hat{\sigma} | el'; n_j+1, n_j'\rangle \\ -\frac{1}{2}\left(n_i + n_j\right)\langle el; n_i, n_i' | \hat{\sigma} | el'; n_j, n_j'\rangle \end{array}\right] + i\hbar\Gamma_A^{rel} \left[\begin{array}{l} \sqrt{n_i'+1}\sqrt{n_j'+1}\langle el; n_i, n_i'+1 | \hat{\sigma} | el'; n_j, n_j'+1\rangle \\ -\frac{1}{2}\left(n_i' + n_j'\right)\langle el; n_i, n_i' | \hat{\sigma} | el'; n_j, n_j'\rangle \end{array}\right] \quad (13)$$

(where the $\Gamma_{\nu\to\nu'}^{rel}$ for K=B,A are given by $\Gamma_{n+1\to n}^{rel} = (n+1)\Gamma_K^{rel}$) [41]. The above Liouville equation is solved with and without the intermediate IR excitation, since at time *t=0* the electronic state is the donor D, and the high frequency oscillators vibrations are in their ground unrelaxed states. To connect with the observables in eqn (1-4), we compute the time evolution of the D and A probabilities with and without the IR perturbation ($P_D(t)$, $P_D^{(IR)}(t)$ and $P_A(t)$, $P_A^{(IR)}(t)$, respectively).

### 2.3.1 Parameter estimates

Eqn (7-13) contain a large number of parameters: the electronic energies and couplings (eqn (7)), the frequencies of the oscillators (eqn (8)), the electron-phonon coupling constants (eqn (9)), the



 

molecule-IR pulse coupling (eqn (10)), and the vibrational decay rates (eqn (13)). This parameter space can be partially reduced because many of the parameters have restricted ranges for typical molecular structures.

In the following we will often compare the electron-vibrational coupling energy, $a_K = -\Delta F_K \sqrt{\hbar/2m_K\omega_K}$ (K=B,A), to the vibrational energy level spacing $\hbar\omega_K$. In particular, $|a_K|/\hbar\omega_K = \sqrt{\lambda_K/\hbar\omega_K} = \sqrt{S_K}$ where $\lambda_K$ is the reorganization energy for charging and $S_K$ is the Huang-Rhys factor for the mode $K$ [42] (Fig. 4b). For high-frequency modes, $|a_K|/\hbar\omega_K < 1$, if we consider typical organic molecular groups (see below).

For the IR field-to-mode coupling strength, $a_{IR} = E_0\left(\partial\mu_{B,IR}/\partial R\right)\sqrt{\left(\hbar/2m_B\omega_B\right)}$, we consider the ratio $|a_{IR}|/\hbar\omega_B$ which is the ratio of the strength to the energy-level spacing between vibrational levels of the mode involved in an IR-induced transition. We can partially constrain $a_{IR}$ by using typical values of $\partial\mu_{B,IR}/\partial R$ for IR-active high-frequency normal modes of organic molecules.

Several parameters of the model are largely system dependent (the electronic site-energies and couplings in eqn (7) and the phonon and electron-phonon parameters in eqn (8) and (9), respectively). These parameters determine the ET mechanism (e.g., deep tunneling, resonant tunneling, or thermally-activated hopping). However their values must be such that the D-to-A ET timescale is of the order of or less than the life time of the excited ET-active IR-active mode, otherwise the excited mode energy will be lost by the time ET takes place. To associate the parameter exploration with ET systems that support fast ET, we consider, the rigid D-$B_n$-A pi-stacked structures of Therien and co-workers [43] as an example. In these systems, the electron donor is a Zn porphyrin, the acceptor a quinone, and the bridge is comprised of a variable number of phenyl rings connected by naphthalene pillars (Fig. 5a). These structures are chosen because the photo-induced D-to-A electron transfer time scale for the single-bridge structure (2a-Zn) and double-bridge structure (3a-Zn) are 600 fs and 3 ps, respectively [43] (of the order of typical lifetimes of high-frequency modes). Further, since we are seeking reversible effects of IR excitation, it is natural to consider rigid systems with high frequency modes that, when excited, do not change the structure of the molecule irreversibly. This condition is also satisfied by the chosen molecular systems. Thus, we imagine adding IR-active oscillators (e.g., CN groups) to the phenyl of the bridge (Fig. 5b) so that one may perform the experiment indicated in Fig. 1 where, e.g., the CN group normal modes are perturbed by IR. We intend to use these CN-modified molecules to derive some of the parameters for the model indicated in eqn (7-10) so that we may explore, on a more realistic footing, if IR excitation of the bridge can significantly perturb the ET kinetics.

We briefly describe the computation of model parameters for the CN-modified 2a-Zn system (denoted as 2a-Zn-CN) in Fig. 5, using DFT implemented in the ADF program [44]. We used the GGA PBE functional with TZ2P basis sets and the frozen core approximation to obtain the energies of the virtual orbitals for the isolated D (porphyrin), B ((naphthalene-phenyl/CN)–napthalene) and A (quinone) fragments of the 2a-Zn-CN molecule. We also used ADF's charge-transfer-integral module to compute the electronic couplings between the virtual orbitals. The energies obtained for the fragment LUMO orbitals and for the electronic couplings between them are shown in Fig. 6 (the fragment LUMO orbitals are shown in Fig. 7). For excited state ET, these LUMO orbitals represent D, possible B and A orbitals for ET. Fig. 6 shows that in these pi-stacked systems, $V_{DB}^{el} \approx V_{AB}^{el} \approx 0.2eV$ and $V_{DB}^{el}/\Delta E_{DB} < 1$ ($V_{AB}^{el}/\Delta E_{AB} < 1$).

To make contact with the experiments in ref [43], we also computed the 2a-Zn-CN molecule's absorption spectrum using TDDFT and compared to experiment using ADF with the same methods as described above. The experimental absorption spectrum for 2a-Zn has a peak centered at $\sim 550nm$ and the excitation that initiates photo-induced ET is centered around this wavelength [43]. The ADF computed spectrum for 2a-Zn-CN contains a sub-band at about $585nm$ and the corresponding excited states contains HOMO-1/HOMO to LUMO+1/LUMO+2 $\pi \rightarrow \pi^*$ excitations localized on the porphyrin subunit of 2a-Zn-CN. These $\pi \rightarrow \pi^*$ states closely resemble the corresponding excited states computed for the isolated porphyrin fragment (Fig. 7, left), and the $\pi$ and $\pi^*$ orbitals involved are very close to the HOMO-1/HOMO and LUMO/LUMO+1 orbitals of the fragment (LUMO and LUMO+1 are energetically very close). Further, the computed minimum energy HOMO to LUMO transition for 2a-Zn-CN involves a $\pi$ orbital HOMO localized at the porphyrin D subunit (very close to the HOMO of the isolated porphyrin fragment), and a LUMO that is localized at the quinone subunit and that is approximately the LUMO of the isolated quinone fragment (Fig. 7 right). Therefore the D, and A orbitals and their energies for 2a-Zn-CN ET are well represented by the values computed for the isolated fragments shown in Fig. 6. The D state is energetically higher than the A state ($E_D^0 > E_A^0$ in Fig. 4), and the B electronic states present a tunneling barrier for ET.

The electron-phonon coupling parameters of our effective model (eqn (9)) will depend on the delocalization of the bridge orbitals occupied by the electron during ET. Although the bridge LUMO shown in Fig. 7 is delocalized over the phenyl ring and the connecting napthalenes, there exist higher-energy bridge virtual orbitals that are more localized on the phenyl ring (these orbitals may also be partially occupied during ET). To obtain indicative values for the electron-phonon coupling parameters for bridge virtual orbitals with different extend of delocalizations, we use the ADF FCF module [45-47]. The module computes modes and normal-mode reorganization energies for electron and hole insertion at the DFT level (using geometry optimization for the neutral and the charged molecules). In our computations of bridge electron-phonon coupling parameters, we use either a bridge fragment that incorporates the central phenyl ring with a CN group and the naphthalene units, or a fragment with just the central phenyl ring with a CN group (all capped with hydrogens). The high frequency normal modes involving CN group vibrations are the same for both bridge fragments and are localized on the phenyl around the CN bond. However, the lowest energy virtual orbital that is occupied by the electron in the anionic bridge fragment used by the ADF computation, (the LUMO of the fragment), has different localizations for the two bridge types. For the larger bridge structure the LUMO is delocalized over the phenyl ring and the naphthalene units (as in Fig. 7). For the smallest bridge structure the LUMO is localized on the phenyl ring (mimicking virtual orbitals of the phenyl ring – naphthalene bridge with energies higher than the bridge LUMO of Fig. 7). This methodology allows us to access a range of

electron-phonon parameter values indicative of electron insertion in delocalized and localized bridge virtual orbitals. We find that for a bridge virtual orbital delocalized over the phenyl and naphthalene rings (Fig 7, middle), the highest $a_B/\hbar\omega_B$ ratio for a CN localized normal mode is $a_B/\hbar\omega_B \approx 10^{-2}$ (where $\hbar\omega_B \approx 0.28eV$, $a_B \approx 0.002eV$, $\lambda_B \approx 2\times10^{-5}eV$). For bridge virtual orbitals that are mostly localized on the phenyl ring, the highest $a_B/\hbar\omega_B$ ratio is $a_B/\hbar\omega_B \approx 0.4$ ($\hbar\omega_B \approx 0.28eV$, $a_B \approx 0.11eV$, $\lambda_B \approx 0.04eV$). We will use this range of parameters in our model. To obtain electron-phonon coupling parameters for the acceptor we use the ADF FCF module using the A (quinone) fragment. We choose the quinone mode with the highest value of the $a_A/\hbar\omega_A$ ratio ($\hbar\omega_A \approx 0.2eV$, $a_A \approx 0.15eV$ and $\lambda_A = 0.11eV$).

The IR field-to-mode coupling strength $a_{IR} = E_0\left(\partial\mu_{B,IR}/\partial R\right)\sqrt{\left(\hbar/2m_B\omega_B\right)}$ (eqn (10)) depends on the electric field strength $E_0$, which is constrained by the laser field characteristics (e.g., laser's repetition rate, energy per pulse, pulse length and diameter etc.). We consider a typical mid-IR pulse setup with a repetition rate $\sim 1KHz$, with energy per pulse of about $10\mu J$, pulse duration $\sigma_{IR} = 100f\,\mathrm{sec}$ and with pulse diameter of about $\sim 50\mu m$. From the power of one pulse and the pulse diameter we can compute the intensity $I$ of the laser beam and then calculate $E_0$ that corresponds to the pulse characteristics (using $I = 0.5\varepsilon_0 cE_0^2$, where $\varepsilon_0$ is the electric permittivity of vacuum, $c$ the velocity of light). By relating $\partial\mu_{B,IR}/\partial R$ to the integrated absorption intensity $A$ of the IR-exited mode, we can obtain the expression $a_{IR} = 1.464\times10^{-11}E_0\sqrt{A/\hbar\omega_B}$ (see Appendix), where $a_{IR}$ and $\hbar\omega_B$ are in units of eV, $E_0$ is in units of V/cm and $A$ in units of km/mole. Both $A$ and $\omega_B$ are computed for the CN localized mode using ADF. The result is $|a_{IR}|/\hbar\omega_B \approx 3\times10^{-2}$ which is quite small, as expected for high frequency modes. However, if we consider the case where the molecular structure is adsorbed and/or located in close proximity to rough metal surfaces, metal island films, or metal particles the molecular IR absorption intensities are significantly changed. This phenomenon of IR absorption enhancement is called "surface-enhanced infrared absorption" (SEIRA) (for a review see [48-50]), and the SEIRA absorption intensity is often expressed as $A_{SEIRA} = A \times f_{SEIRA}$, where $f_{SEIRA} = 10-1000$. Therefore, the SEIRA effect allows greater flexibility on varying the magnitude of $a_{IR}$ in an experiment, $a_{IR} = 1.464\times10^{-11}E_0\sqrt{f_{SEIRA}A/\hbar\omega_B}$. In the following we use a conservative value $f_{SEIRA} \approx 40$ to bring $a_{IR}$ up to magnitudes that could be accessible by SEIRA experiments. For high-frequency CN modes this enhancement gives $|a_{IR}|/\hbar\omega_B \approx 0.2$. Since we are considering SEIRA experiments, we have to allow the possibility of fast vibrational relaxation of the IR-excited mode in the simulations. Therefore, we vary $1/\Gamma_B^{rel}$ from sub-ps (100 fsec) to ps values.

### 2.3.2 Parameter search

To summarize we have obtained a set of model parameter values for a class of DBA ET systems that performs fast (sub-ps to ps) photo-induce ET. These values will be used as a starting point for our numerical exploration of IR-perturbed ET. Using our model (eqn (7-11)) we compute $P_K(t)$, $P_K^{(IR)}(t)$ (K=D,B,A), and the integrals $\int_0^T dtP_K(t)$ and $\int_0^T dtP_K^{(IR)}(t)$ (K=D,A) that are necessary for computing yields. The time T in the integrals is the time required for the IR-perturbed D, B, and A probabilities to return to their unperturbed values (this always happens since the IR pulse is of finite width). In the examples shown in the figures, we report the fractional changes in D and A yields computed over finite times T,

$$I_D = \frac{\int_0^T dtP_D^{(IR)}(t) - \int_0^T dtP_D(t)}{\int_0^T dtP_D(t)}, \quad (14a)$$

$$I_A = \frac{\int_0^T dtP_A^{(IR)}(t) - \int_0^T dtP_A(t)}{\int_0^T dtP_A(t)} \quad (14b)$$

Large values of $I_K$ suggest that the IR perturbations of the ET rates can be observed via yield measurements of reactions that involve either D or A. The IR pulse is always applied during the ET event. We choose the initial state with electron on D and the oscillators in their unrelaxed ground states ($|D\rangle|0_B^u\rangle|0_A^u\rangle$). For the final state, the electron is transferred fully to A, the bridge oscillator is in an unrelaxed state, and the acceptor oscillator in a relaxed state ($|A\rangle|n_B^u\rangle|n_A^R\rangle$). In all computations we maintain initial state to final state resonance which ensures that the unperturbed (without IR perturbation) ET rate is of ~ps timescale. Further , in eqn (10), the pulse width $\sigma_{IR}$ is ~100 fs and $|a_{IR}|/\hbar\omega_B$ can vary between 3x10$^{-2}$ and ~0.2 (the minimum value mimics a solution-phase experiment and the maximum value, a SEIRA experiment with ~ 40 times enhancement, see Appendix). $|a_B|/\hbar\omega_B$ can vary between ~10$^{-2}$ and ~0.5 (delocalized versus localized bridge orbitals).

### 2.3.3 Discussion

Our simulations show that the effect of IR on the D, B and A probabilities and on the ET yields (eqn (14)) is negligible for the parameters derived from the computations on 2a-Zn-CN, even for high $|a_{IR}|$ values compatible with SEIRA experiments and for the highest $|a_B|$. This is mainly due to the fact that the B LUMO is off-resonant to the D LUMO, thus creating a tunneling barrier for the electron as it transfers from D to A (Fig. 6). Therefore, the transferring electron does not occupy the bridge with high probability, and the IR excitation of the B oscillator (eqn (10)) cannot perturb ET even with very strong surface-enhanced fields. A design solution to produce stronger IR perturbations on ET is to change the D, B or A moieties so that the B LUMO energy lies between D and A LUMO energies in order to obtain energetic resonance $\left(E_D^0 > E_B^0 > E_A^0\right)$. In this case it is expected that the transferring electron will occupy the bridge with high probability. Several examples of this regime are discussed below.



 

Fig. 8 shows the time evolution of the D, B and A probabilities with and without IR for the parameters derived from the computations on 2a-Zn-CN (Figs. 5-6) and with a large $|a_{IR}|/\hbar\omega_B \approx 0.2$. In the simulation we have set $E_D^0 > E_B^0 > E_A^0$ to mimic the regime of ET where the bridge electronic states can be occupied by the transferring electron with high probability. The vibrational relaxation time is 1 ps and $V^{el}/\hbar\Gamma_B^{rel} >> 1$ ($V_{DB}^{el}/\hbar\Gamma_B^{rel} \approx 333$ and $V_{AB}^{el}/\hbar\Gamma_B^{rel} \approx 338$). The effect of the IR pulse on the yields is 10-65%. Therefore, if the B orbital energy is brought within the D-A energy gap, $\left(E_D^0 > E_B^0 > E_A^0\right)$, the IR-perturbation on the D and A yields can be substantial. This energy shifting can be achieved in the context of our model compound by adding substituents to the porphyrin ring or to the bridge. For example, we performed ADF computations using the GGA PBE functional with TZ2P basis, to confirm that the bridge LUMO energy can be tuned between the D and A LUMO energies by substituting electron-withdrawing groups (e.g., -$NO_2$,-CHO,-CN,-$CF_3$) on the phenyl ring. Similarly, the D LUMO can be lifted above the B LUMO by substituting electron-donating groups on the porphyrin (e.g., -$NH_2$,-$CH_3$,-$OCH_3$) [51].

To demonstrate the robustness of the above result to changes in system parameters, Figs. 9 and 10 show the same system as in Fig. 8 with a vibrational relaxation time of 1 ps, but with different values for the electronic couplings that lower the ratios of $V^{el}/\hbar\Gamma_B^{rel}$ while maintaining $V^{el}/\hbar\Gamma_B^{rel} > 1$. We see that ET-perturbation effect is relatively robust to changes in $V^{el}$ in the regime $V^{el}/\hbar\Gamma_B^{rel} > 1$, especially with respect to $I_D$. Further, if the electronic couplings are unsymmetric ($V_{DB}^{el} \neq V_{AB}^{el}$) the IR-perturbation to the D yield can be enhanced up to 40% for short IR-pulse delay times $t_0$ (Table I).

Fig. 11 shows the influence of faster-than-psec vibrational relaxation of the B oscillator ($1/\Gamma_B^{rel} = 164\,fs$), keeping the other parameters of the system as in Fig. 8. In this case, the electronic couplings are symmetric and $V_{DB}^{el}/\hbar\Gamma_B^{rel} \approx 60, V_{AB}^{el}/\hbar\Gamma_B^{rel} \approx 60$. The effect of increasing the vibrational relaxation rate while keeping $V^{el}/\hbar\Gamma_B^{rel} > 1$ is to enhance the IR perturbation for the D yield to values close to 70% ($I_D \approx 0.7$, $I_A \approx -0.1$). This enhancement is robust with respect to the IR-pulse delay time (Table II). Fig. 12 shows the same system as in Fig. 11 where the A-B coupling is reduced to introduce a coupling asymmetry ($V_{DB}^{el}/\hbar\Gamma_B^{rel} \approx 60$ and $V_{AB}^{el}/\hbar\Gamma_B^{rel} \approx 5$). The asymmetry, as in the case of Fig. 10 (Table I), enhances the yields with $I_D \approx 0.93$ and $I_A \approx -0.19$. The IR perturbations are largely independent of the IR-pulse delay times (Table III).

In the above simulations, the ratio of $V_{DB}^{el}/\hbar\Gamma_B^{rel}$ and $V_{AB}^{el}/\hbar\Gamma_B^{rel}$ are greater than unity. This is due to the relatively high coupling values (imposed by the pi-stacking DBA arrangements in the molecules used as an example), and the sub-ps to ps lifetime of the bridge CN vibrational mode excited by IR. If these ratios are reduced, the effect of the IR on the D and A yields is also reduced. In Fig. 13, we show the effect of reducing the $V^{el}/\hbar\Gamma_B^{rel}$ ratios to values less than 1 (the other parameters are the same as in Figs. 11 and 12). The IR- perturbation to the ET yields drops to 10% and 4% for D and A respectively (eqn (14)). Table IV shows that the 10% perturbation persists for all time delays of the IR pulse.

A general trend is observed in Figs. 8-13 if we define the ET time scale $\tau_{ET}$ to be approximately the time when the unperturbed acceptor probability passes through ~50% ($P_A \approx 0.5$), and we compare this time to the vibrational relaxation time of the IR-perturbed B mode, $\tau_B^{rel} \approx 1/\Gamma_B^{rel}$. For Figs. 8, 10, 11 and 12, $\tau_B^{rel} \approx \tau_{ET}$ (the time scales of ET and vibrational relaxation are of the same order), and for Figs. 9 and 13, $\tau_B^{rel} < \tau_{ET}$ (the vibrational relaxation of the B mode is faster than ET). In Figs. 8,10,11 and 12 the application of the IR perturbation targeting the B mode leads to significant IR effect on the D, A populations and the yields ($I_D \sim 0.1-0.96,\ I_A \sim 0.01-0.22$). In contrast, in Figs. 9 and 13, the IR-perturbation effect is much smaller ($I_D \sim 0.01-0.15,\ I_A \sim 0.01-0.05$).

In general, our simulations indicate that IR perturbations of ET yields can be substantial if the electron-vibrational coupling is significant (up to the realistic value of $|a_B|/\hbar\omega_B \approx 0.5$) and the transport mechanism is coherent resonant through-bridge tunneling with $V^{el}/\hbar\Gamma_B^{rel} > 1$, provided that the IR-perturbation is strong (e.g., $|a_{IR}|/\hbar\omega_B \approx 0.2$). Such strong IR perturbation is readily achievable via SEIRA experiments. It should be noted that the ratio $|a_B|/\hbar\omega_B$ is never taken to values much greater than unity because this would give unrealistic electron-vibrational coupling constants $a_B$ given that $\hbar\omega_B$ is always a few tens of an eV (as we are considering high frequency ET-active modes that lie above the mode continuum).

In summary, we have shown that in D-B-A systems where the ET mechanism is coherent resonant tunneling, the ET rate can be perturbed during electron transfer by IR excitation of a high-frequency B ET-active mode. The ET rate perturbation is enhanced if the ET system's D-B and A–B electronic couplings are large enough such that the overall ET time is of the order of the vibrational relaxation time of the system's IR-perturbed mode. These conditions are valid for systems with realistic electron-vibrational coupling values ($|a_B|/\hbar\omega_B \leq 1$), and they can give up to 100% changes in the ET yields if the IR-pulse perturbation is strong, within the limits that can be achieved by SEIRA experiments.

### 2.4 IR perturbation of slow ET rates with low-frequency ET-active vibrations

The typical vibrational-relaxation and energy-redistribution times of excited vibrational modes in molecules are sub-ps to a few ps. Most bridge-mediated ET time scales are much longer than ps. In this regime of slow ET (slow with respect to vibrational relaxation), bridge ET-active modes (modulating B electronic state energies and/or D-B (A-B) electronic couplings) may have periods much slower than psec. Such "low frequency" ET-active modes lie deep in the mode continuum of the molecule and are very difficult to excite directly and selectively by IR. Even if these modes could be excited, they are likely to lose their excess energy to the mode continuum on a very fast time scale (sub-ps). Therefore, to perturb the ET rate

using the low-frequency ET-active modes, the latter must serve as a sink of excess energy supplied to the system via other high-frequency modes that can be selectively excited by IR. ET must be initiated when the excess vibrational energy has reached the ET-active modes, such that the ET reaction will take place in a nonequilibrium ensemble of these modes. Further, the ET-active modes should be able to retain the excess energy for a sufficiently long time to sustain the nonequilibrium ET ensemble.

To illustrate this point, consider bridge-mediated ET where the ET mechanism is through-bridge elastic tunneling and the ET timescales are much longer than ps [1,2,11]. Often, the bridge-mediated D-A coupling is very sensitive to bridge vibrations [52,53], e.g., when the relevant electron-tunneling pathways contain through-space or hydrogen bond steps with a range of thermally accessible distances (i.e., soft vibrations) [9-12,54,55]. In this case, where access to a wide range of structures is possible and the time scale of interchange is rapid, the rate is given by $k_{D\to A} = (2\pi/\hbar)\langle T_{DA}^2\rangle_{eq}\rho_{FC}$, where $\rho_{FC}$ is the Franck Condon factor and $\langle T_{DA}^2\rangle_{eq}$ is the thermal equilibrium average of $T_{DA}^2$. Consider high-frequency IR-active modes that transfer excess energy to the ET-active modes that modulate $T_{DA}$ (when the former are excited by IR) on a time scale $\tau_{IVR}$ (Fig. 14a). If ET is initiated at a time $\tau_{IVR}$ after IR excitation, the ET rate is $k_{D\to A}^{(IR)} = (2\pi/\hbar)\langle T_{DA}^2\rangle_{neq}\rho_{FC}$, where $\langle T_{DA}^2\rangle_{neq}$ is an average over a nonequilibrium ensemble (with respect to the ET-active modes) which modulates the D-A coupling (Fig. 14b).

Therefore, in this slow ET rate regime, the design of an experiment that produces IR modulation of ET rates will depend critically on the details of molecular structure. The ET system must have vibrations that modulate ET pathways, and these vibrations must also be sinks for the excess energy supplied to the system by the excitation of high-frequency IR-active modes. It is thus essential to have computational tools that can identify the molecular electron tunneling pathways, the ET-active modes that modulate them, the IVR pathways that deactivate the ET-active modes, and the corresponding IVR timescales, $\tau_{IVR}$. The computation of time-dependent tunneling pathways and $\langle T_{DA}^2\rangle_{eq}$ is quite familiar [10], but the computation of IVR pathways and IVR time scales remains a challenging task [38-40]. Combining electron tunneling and IVR pathway design in order to maximize $\langle T_{DA}^2\rangle_{neq}$ is possible in the context of classical nonequilibrium molecular dynamics simulations (that model the effect of IR excitation) coupled to electronic structure computations on DBA structures derived from the nonequilibrium ensemble (a subject of a future paper [56]).

## Conclusions

Previous theoretical studies of IR-pulse control of ET rates [21-24] motivated experiments on small D-B-A systems that demonstrate ET rate modulation is possible by targeting specific bridge ET-active modes [25,27]. These experiments showed different levels of IR-induced modulation and the challenge now is to understand the parameter regimes that determine the magnitude of the effect and to suggest systems and experimental setups that optimize ET rate control. Another central challenge is to understand the influence of vibrational energy redistribution (and dephasing) which is likely to diminish the influence of vibrational excitation of ET-active modes on ET rates and yields. To this end, we have explored the feasibility of perturbing bridge-mediated ET by exciting ET-active bridge vibrations with a single IR pulse using a density matrix (Lindbland-type) model that takes into account vibrational relaxation. We also presented experimental observables, pulse sequences and molecular architectures that may enable measurement of IR-pulse perturbations to bridge-mediated ET rates. The suggested molecular architectures may also allow for control of ET pathways in D-B-A systems via selective IR excitations of bridge modes.

In this context, we explored two scenarios for IR control, one for slow nonadiabatic ET rates (slower than vibrational relaxation times) and the other for fast ET rates (of the order of vibrational relaxation times). The main focus of this study is the fast ET rate regime (~ ps) where the aim is to perturb ET "as the electron transfers" by directly exciting an IR-active ET-active bridge mode with subpsec period and a frequency above the mode continuum. In this fast ET regime, vibronic coherences are likely to influence ET as long as the solvent environment does not destroy such coherences on time scales faster than the ET time scale. In this situation the IR perturbation changes the ET rate by directly affecting these coherences.

We find that two important generic conditions need to be satisfied in order to have any measurable IR-perturbing effect on the ET rate "as the electron transfers". First the B electronic state must be occupied with substantial probability during ET. Since the IR pulse weakly perturbs the bridge oscillator, and the bridge oscillator interacts with the occupied B electronic state, the state should have large occupation during ET in order to perturb ET sufficiently with IR. This means that the B state cannot be a deep tunneling barrier for the transferring electron as in that case there is negligible population buildup of this state during ET. The second condition relates to the competition between vibrational relaxation and ET. If the timescale of ET into B (from D) and out of B (to A) is slower than typical vibrational relaxation times of the B oscillator excited state, then effects of the IR pulse on ET as the electron transfers will be diminished. By the time ET to (and from) the bridge takes place the IR-excited oscillator will have relaxed to the ground state and the IR pulse will not influence ET.

This condition can be roughly described as follows: if the D-B system is isolated by turning off the B-A electronic coupling then the D-to-B ET timescale should be comparable to or shorter than the B oscillator vibrational relaxation timescale. The same should hold for the B-to-A ET time scale if the B-A system is isolated by turning off the D-B electronic coupling. It must be emphasized that in this work we are not analysing a simple activation (heating) effect of the IR pulse. Namely, if B vibrational relaxation is fast and it takes place before ET from B-to-A, then an IR pulse applied to B after vibrational relaxation could activate ET to A. The regime studied here is different; it is the IR-pulse perturbation (disturbance) of coherent ET prior to or during vibrational relaxation.

The observations above suggest that the IR-perturbation effect is maximized for coherent resonant tunneling. For typical and moderate bridge electron-vibrational couplings, the IR-perturbation effect is substantial only for relatively strong IR fields that are accessible via surface enhanced infrared absorption settings. An alternative to surface enhanced IR for augmenting the vibrational excitation of the bridge (albeit less specifically) is to attach heat source molecules to the bridge [57]. These molecules (e.g., azobenzene) undergo rapid internal conversion when excited



 

electronically, damping the excess electronic energy to neighboring vibrations.

For the slow ET rate regime modulated by low-frequency ET-active bridge modes, IR-excitation of high frequency bridge modes should be designed to change the thermal ET ensemble to a nonequilibrium ensemble of the ET-active modes. This is possible only if the ET-active modes serve as a sink for the excess vibrational energy supplied by the IR-pulse. Alternatively it is interesting to explore whether THz pulses that directly excite the low frequency ET active modes can be used to perturb ET. Designing ET systems with such characteristics requires realistic simulations of IVR pathways coupled to ET pathways, and such simulation protocols are the subject of a follow up paper.

## Appendix

An ultrafast pulsed laser periodically emits pulses of energy, with a specific repetition rate, of ultra-short time duration [58] (Fig. A1). Typical mid-IR pulses of interest can be generated with a repetition rate $\sim 1KHz$ (a pulse every *1msec*, Fig. A1), with energy per pulse of about $1-10\mu J$ and pulse duration $\sigma_{IR}=100\,f\,\text{sec}$ and with pulse diameter of about $\sim 50\mu m$. In the D-B-A systems under study the ET time scale is of order ps. After ET initiation, and within a ps time interval, we assume that one IR pulse can be applied, centered at $t_0$ (where $t_0=\tau$ in eqn (10)). In order to calculate the power of one pulse, we divide the generated pulse energy with the pulse duration, which is described by its width $\sigma_{IR}$. From the power of one pulse and the pulse diameter we can compute the intensity $I$ of the laser beam (power per unit area). The intensity is then set equal to $I=0.5\varepsilon_0 cE_0^2$ , where $\varepsilon_0$ is the electric permittivity of vacuum, $c$ the velocity of light and $E_0$ is an average of the electric field strength. Using this latter equation and the previously computed value of $I$ we can derive a value for $E_0$ in units V/cm that corresponds to the pulse characteristics.

If we assume Beer's law and $I=I_0e^{-aC\ell}$, the integrated absorption intensity of an infrared transition is defined as [59]:

$$A=\int_{band} a(\nu)d\nu=\frac{1}{C\ell}\int_{band}\ln\left(\frac{I_0}{I}\right)d\nu \qquad \text{(A1)}$$

where $I_0$ is the intensity of radiation incident on the sample at wavenumber $\nu$, $I$ the transmitted intensity, $a$ is the absorptivity, $C$ is the sample concentration and $\ell$ the path length. The range of integration is over a spectral region of interest.

The integrated absorption intensity of the ith fundamental vibrational band, $A_i$ in $km/mole$, is related to the dipole moment derivative with respect to the ith mass-weighted normal mode coordinate, $Q_i$ by [44,59,60]:

$$A_i=\frac{1}{4\pi\varepsilon_0}\frac{N_A\pi g_i}{3c^2}\left(\frac{\partial\mu_{IR}}{\partial Q_i}\right)^2 \qquad \text{(A2)}$$

where $N_A$, $c$ and $g_i$ are Avogadro's number, the velocity of light and the degeneracy of the ith band, respectively, and $4\pi\varepsilon_0$ permits use of SI units.

In our models we have defined the IR pulse perturbation as (eqn (10)) $a_{IR}=E_0\left|\partial\mu_{B,IR}/\partial R\right|\sqrt{\left(\hbar/2m_B\omega_B\right)}$. Using eqn (A2) where $Q_i=\sqrt{m_B}R$ to solve for $\left|\partial\mu_{B,IR}/\partial Q_i\right|$, and substituting into $a_{IR}$, gives

$$a_{IR}=1.464\times10^{-11}E_0\sqrt{A_i/\hbar\omega_B} \qquad \text{(A3)}$$

in units of eV.

We use this equation to compute $a_{IR}$ with the value of $E_0$ as derived from the pulse characteristics above, and with $A_i$ and $\hbar\omega_B$ values computed for the CN normal mode of interest using the ADF normal mode module. This gives the lowest limit of $a_{IR}/\hbar\omega_B\approx3\times10^{-2}$.

To obtain upper limits for $a_{IR}/\hbar\omega_B$ we consider the surface enhancement infrared absorption (SEIRA) effect. This effect is described by introducing an enhancement factor for the molecule's specific absorption intensity $\left(A_i^{SEIRA}=A_i f_{SEIRA}\right)$, where $f_{SEIRA}\approx10-1000$. Therefore, taking into account the SEIRA effect,

$$a_{IR}=1.464\times10^{-11}E_0\sqrt{\left(f_{SEIRA}\times A_i\right)/\hbar\omega_B}\,. \qquad \text{(A4)}$$

where $a_{IR}$ and $\hbar\omega_B$ are in units of eV, $E_0$ is in units of V/cm and $A_i$ in units of km/mole. In this work we use $f_{SEIRA}\approx40$ (a conservative value) to obtain the upper limit of $a_{IR}/\hbar\omega_B\approx0.2$.

## Acknowledgements

The authors thank the Cyprus Research Promotion Foundation for financial support of the project via the research Grant "Vibrational Control of Electron Transfer, ΔΙΕΘΝΗΣ ΣΤΟΧΟΣ-0311/04." The authors thank Dr D. Tsokkou and Profs. A. Keramidas, A. Othonos, I.V. Rubtsov, M. J. Therien, A. Vlček T. and W. Zinth, for helpful and insightful discussions.

## Notes and references

[a] Department of Physics University of Cyprus, Nicosia 1678, Cyprus.
[b] Department of Chemistry, Duke University, Durham, North Carolina, 27708 USA.
[c] Department of Physics, Duke University, Durham, North Carolina, 27708 USA.
[d] Department of Biochemistry, Duke University, Durham, North Carolina, 27708 USA.

[e] Freiburg institute of Advanced Studies (FRIAS), University of Freiburg, 79104 Freiburg, Germany.

[1] R.A. Marcus and N. Sutin, *Biochim. Biophys. Acta*, 1985, **811**, 265–322.
[2] J.R. Winkler and H.B. Gray, *Biochim. Biophys. Acta*, 2010, **1797**, 1563–1572.
[3] J. Jortner and M. Bixon, Electron Transfer: From Isolated Molecules to Biomolecules, Adv. Chem. Phys. Ser. 106–107, New York, Wiley Intersci. eds. 1999.
[4] V. Balzani, P. Piotrowiak, MAJ Rodgers,J. Mattay, D. Astruc, et al. 2001. Electron Transfer in Chemistry, Vols. I–V.Weinheim:Wiley-VCH
[5] A. Nitzan, Chemical Dynamics in Condensed Phases, Oxford Univ. Press: Oxford, 2006.
[6] V. May and O. Kuhn, Charge and Energy Transfer Dynamics in Molecular Systems, Wiley-VCH, Berlin, 2000.
[7] D.N. Beratan and S.S. Skourtis, *Curr. Op. Chem. Biol.*, 1998, **2**, 235-243.
[8] S.S. Skourtis and D.N. Beratan, *Adv. Chem. Phys.*, 1999, **106**, 377–452.
[9] S.S. Skourtis, J. Lin and D.N. Beratan, In Modern Methods forTheoretical Physical Chemistry of Biopolymers, edited by E.B. Starikov, J.P. Lewis and S. Tanaka, Elsevier: Boston, MA, 2006.
[10] D.N. Beratan, S.S Skourtis, I.A. Balabin, A. Balaeff, et al., *Acc. Chem. Res*., 2009, **42**, 1669–1678.
[11] S.S. Skourtis, D.H. Waldeck and D.N. Beratan, *Annu. Rev. Phys. Chem.*, 2010, **61**, 461–485.
[12] S.S. Skourtis, *Biopolymers (Peptide Science)*, 2012, **100**, 82-92.
[13] D. N. Beratan, C. Liu, A. Migliore, N. F. Polizzi, S. S. Skourtis, P. Zhang, and Y. Zhang, *Acc. Chem. Res., Articles ASAP Publication* Date (Web): October 13, 2014 (Article) DOI: 10.1021/ar500271d.
[14]Y. Zhang, L. Chaoren Liu, A. Balaeff, S.S. Skourtis, and D. N. Beratan, *Proc. Natl. Acad. Sci. USA*, 2014, **111** (28), 10049-10054 .
[15] F. Fassiolo, R. Dinshaw, P.C. Arpin, and G.D. Scholes, *J. R. Soc. Interface*, 2013, **11,** 20130901.
[16] M. Mohseni, Y. Omar, G. Engel and M. Plenio, Quantum Effects in Biology, Cambridge University Press, 2014.
[17] I. Gideon, G. I. Livshits, A. Stern, D. Rotem, et al., *Nature Nanotechnology*, 2014, **9**, 1040-1046.
[18] A. de la Lande, J. Řezáč, B. Lévy, B. C. Sanders, and D. R. Salahub, J. *Am. Chem. Soc*., 2011, **133** (11), 3883-3894.
[19] E. Romero, R. Augulis, V. I. Novoderezhkin, M. Ferretti, J. Thieme, D. Zigmantas and R. van Grondelle, *Nature Physics*, 2014, **10**, 676–682
[20] F. D. Fuller, J. Pan, A. Gelzinis, V. Butkus, S. Seckin Senlik, D. E. Wilcox, C. F. Yocum, L.Valkunas, D. Abramavicius and J. P. Ogilvie, *Nature Chemistry*, 2014, **6**, 706–711
[21] S.S. Skourtis, D.H. Waldeck and D.N. Beratan, *J. Phys. Chem. B*, 2004, **108**, 15511–15518.
[22] S.S. Skourtis and D.N. Beratan, *AIP Conf. Proc*., 2007, **963**, 809–812.
[23] D. Xiao, S.S. Skourtis, I.V. Rubtsov and D.N. Beratan, *Nano Lett.*, 2009, **9**, 1818–1823.
[24] H. Carias, D.N. Beratan and S.S. Skourtis, *J. Phys. Chem. B*, 2011, **115**, 5510-5518.
[25] Z. Lin, C.M. Lawrence, D. Xiao, V.V. Kireev, et al., *J. Am. Chem. Soc*., 2009, **131**, 18060–18062.
[26] R.A. Goldsmith, M.R. Wasielewski and M.A. Ratner, *J. Phys. Chem*., 2006, **110**, 20258-62.
[27] M. Delor, P.A. Scattergood, I.V. Sazanovich, A.W. Parker, G.M. Greetham, A. J. H. M. Meijer, M.Towrie, and J. A. Weinstein, *Science* 2014, **346**, (6216) 1492-1495.
[28] Y. Yue, T. Grusenmeyer, Z. Ma, P. Zhang, R. H. Schmehl, D. N. Beratan and I. V. Rubtsov, *Dalton Trans.* 2015, Advance Article **DOI:** 10.1039/C4DT02145B
[29] M. Fedoseeva, M. Delor, S.C. Parker, I.V. Sazanovich, M. Towrie, A. W. Parker and J. A. Weinstein, *Phys Chem Chem Phys*, 2015 **17**, 1688-1696.
[30] M. Delor, I.V. Sazanovich, M. Towrie, S. J. Spall, T. Keane, A. J. Blake, C. Wilson, A. J. Meijer and J. A. Weinstein, *J Phys Chem B*, 2014,**118**, 11781-11791.
[31] M. Delor, I. V. Sazanovich, M. Towrie, and J. A. Weinstein, *Acc. Chem. Res.*, Articles ASAP Publication Date (Web): March 19, 2015 (Article) **DOI:** 10.1021/ar500420c
[32] A. Vlček, Jr., H. Kvapilová, M. Towrie, and S. Záliš, *Acc. Chem. Res.*, 2015, **48**, 868–876
[33] T. A. A. Oliver, N. H. C. Lewis, G.R. Fleming *Proc. Natl. Acad. Sci. U. S. A.* 2014, **111**, 10061–10066.
[34] J. L. Miller, *Physics Today*, 2015, **68**, 10-11
[35] D.G. Evans, R.D. Coalson and Y.J. Dakhnovski, *Chem. Phys*., 1996, **104**, 2287-2296.
[36] S. Kohler, J. Lehmann and P. Hanggi, *Phys. Rep*., 2005, **406**, 379–443.
[37] I. A. Solov'yov, T. Ritz, K. Schulten and P. J. Hore, In Quantum effects in biology', ed. M. Mohseni, Y. Omar, G. Engel and M. Plenio, Cambridge University Press, 2014.
[38] H. Fujisaki and J.E. Straub, *Proc. Natl. Acad. Sci.*,U.S.A., 2005, **102**, 6726–6731.
[39] G. Stock, *Phys. Rev. Lett*., 2009, **102**, 118301.
[40] D.M. Leiner, *Annu. Rev. Phys. Chem*., 2008, **59**, 233-59.
[41] G. Li, B. Movaghar, A. Nitzan and M.A. Ratner, *J. Chem. Phys*, 2013, **138**, 044112.
[42] P. F. Barbara, T. J. Meyer and M. A. Ratner *J. Phys. Chem*., 1996, **100**, 13148–13168
[43] Y.K. Kang, P.M. Iovine, and M. J. Therien, *Coord. Chem. Rev*., 2011, **255**, 804-24.
[44] G.T. Velde, F.M. Bickelhaupt, E.J. Baerends, C.F. Guerra, S.J.A. Van Gisbergen, J.G. Snijders, and T. Ziegler, *J. Comp. Chem*., 2001, **9**(22), 931-967.
[45] J.S. Seldenthuis, H.S.J. van der Zant, M.A. Ratner and J.M. Thijssen, *ACS Nano*, 2008, **2**(7), 1445-1451.
[46] G.M. Sando and K.G. Spears, *J. Phys. Chem. A*, 2001, **105**, 5326-5333.
[47] P.T. Ruhoff and M.A. Ratner, *Int. J. of Quantum Chem.*, 2000, **77**, 383-392.
[48] M. Osawa, In Near-Field Optics and Surface Plasmon Polaritons, edited by S.Kawata, Topics Appl. Phys.,2001, 81, 163–187, Springer-Verlag Berlin Heidelberg.
[49] F. Siebert and P. Hildebrandt, Vibrational Spectroscopy in Life Science, WILEY-VCH, 2008.
[50] R. Aroca, Surface-Enhanced Vibrational Spectroscopy, Wiley, 2006.
[51] W. A. Goddard, D. W. Brenner, S. E. Lyshevski and G. J. Iafrate, Handbook of Nanoscience, Engineering, and Technology, CRC Press, 2003.
[52] S.S. Skourtis, Q. Xie and G. Archontis, *J. Chem. Phys*., 2001, **115**, 9444–9462.
[53] A. Teklos and S.S. Skourtis, *Chem. Phys*., 2005, **319**, 52–68.
[54] S.S. Skourtis, I.A. Balabin, T. Kawatsu and D.N. Beratan, *Proc. Natl. Acad. Sci. U.S.A.*, 2005, **102**, 3552–3557.
[55] I.A. Balabin, D.N. Beratan and S.S. Skourtis, *Phys. Rev. Lett.*, 2008, **101**,158102.
[56] M. Zheng, P. Antoniou, P. Zhang, S.S. Skourtis and D.N. Beratan, Vibrational Control of Electron Transfer Reactions II: A Non-Equilibrium Molecular Dynamics Study. To be submitted.
[57] W.J. Schreier, T. Aumüller, K. Haiser, F.O. Koller, M. Löweneck,H-J Musiol, T.E. Schrader, T.Kiefhaber, L. Moroder, and W. Zinth, Peptide *Science (Biopolymers)*, 2013, **100**, 38-50.
[58] C. Rullière, Femtosecond Laser Pulses Principles and Experiments, Second Edition, Springer, 2005.
[59] W.B. Person and G. Zerbi, Vibrational Intensities in Infrared and Raman Spectroscopy, Elsevier, 1982.
[60] ADF Manual, ADF Program System 2013.



 

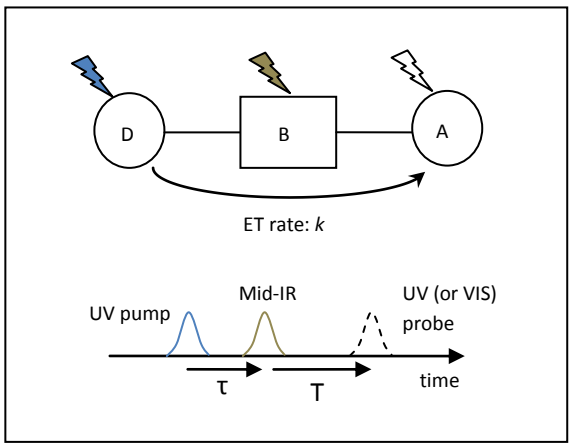


**Fig. 1** DBA ET where a UV (VIS) pulse excites the D electronic state initiating ET to the A state, and an IR pulse excites selected B vibrational modes. The final A state population is either probed by another UV(VIS) pulses or indirectly if A is involved in a chemical reaction whose rate is measurable.

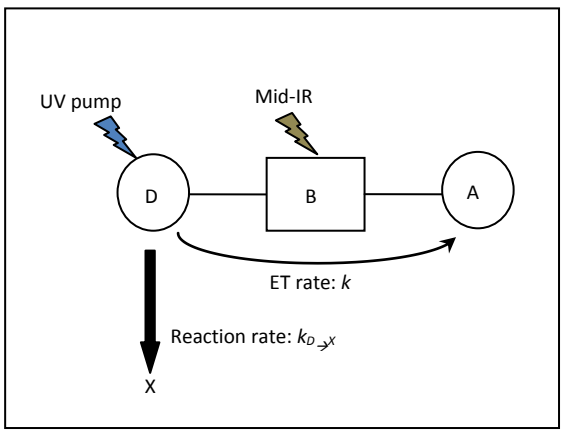


**Fig. 2** DBA ET where a UV (VIS) pulse excites the D electronic state initiating ET to the A state, and an IR pulse excites selected B vibrational modes. The D state is involved in a competing chemical reaction that produces the product X. By measuring the fractional change upon excitation with IR of the infinite time yield of this reaction it is possible to deduce the fractional change in the ET rate induced by IR (eqn (1)).

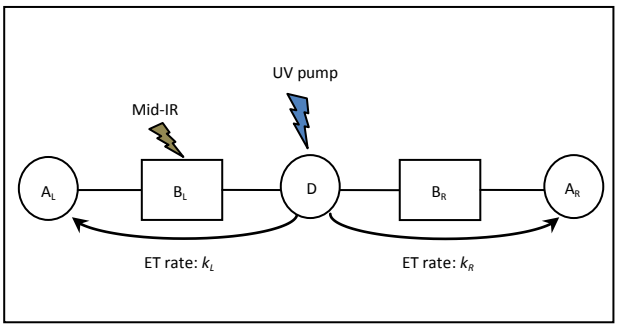


**Fig. 3** A D moiety connected via left and right B units ( $B_L$ , $B_R$ ) to A moieties ( $A_L$ , $A_R$ ). Upon photo-excitation of D, irreversible ET is initiated simultaneously to $A_L$ and to $A_R$ (with ET rates $k_L$ and $k_R$ ). For this system architecture, the IR excitation of one B unit can irreversibly affect the directionality of ET. In addition, the asymmetry in the infinite-yields of the $A_L$ and $A_R$ can give a direct measure of the IR perturbation of the ET rate.

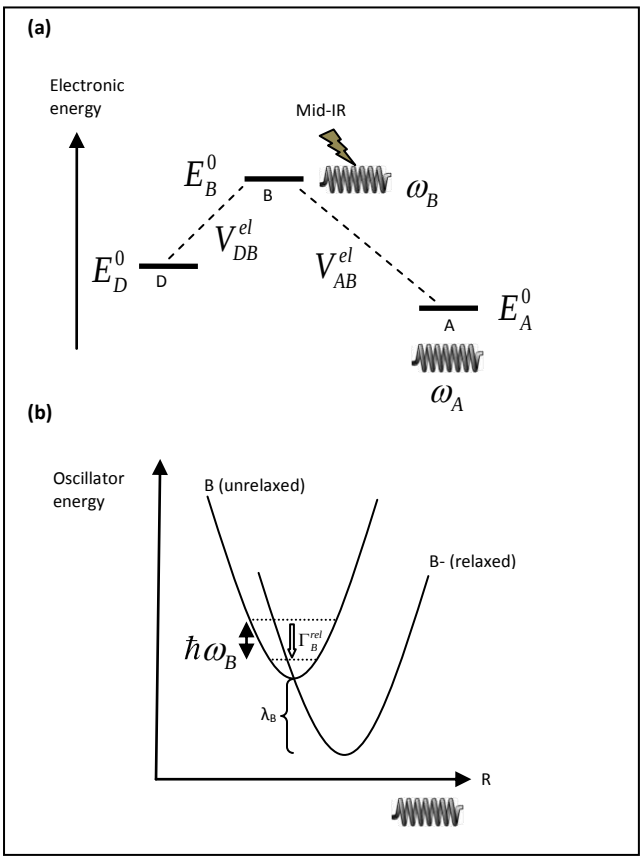


**Fig. 4 a)** Schematic diagram of the model system in eqn (7-13). The system is comprised of a D, B and A electronic state and two oscillators, one coupled to the B state and the other to A state. **b)** Diagram showing that the oscillator-electronic state coupling is linear. The oscillator state dynamics is dissipative with vibrational relaxation rates $\Gamma_{\nu\to\nu'}^{rel}$. In this work we focus on fast coherent ET, where the ET rate is of the order of the vibrational relaxation rates.

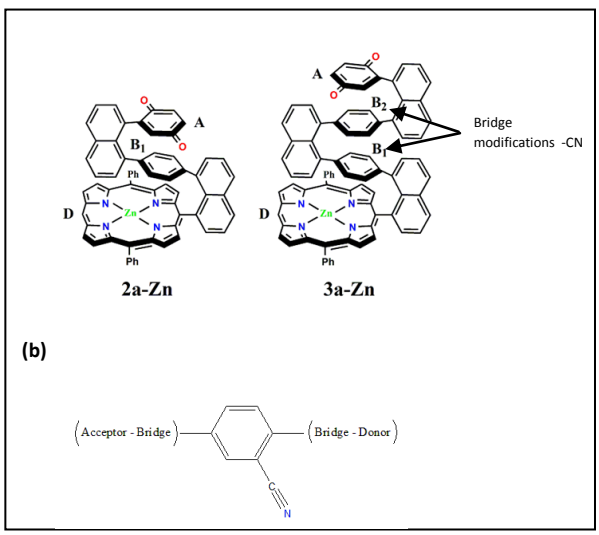


**Fig. 5 a)** The pi-stacked D-B-A systems that are used as a case study for photo-induced ET. The Zinc-porphyrin is the donor the bridge is comprised of phenyl rings connected by naphthalene units and the acceptor is quinone [43]. Photo-induced ET rates are 600 fsec for 2a-Zn and 3 psec for 3a-Zn. We envisage adding IR active groups to the bridge units such as CN in order to

probe for IR perturbed ET (e.g., as in Fig. 1). b) A CN group substitution to the phenyl of the bridge.

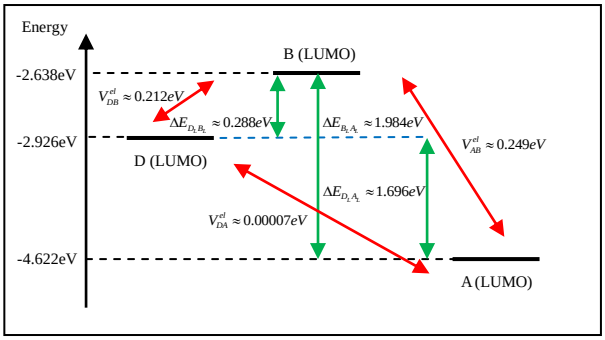


**Fig. 6** Energies of LUMO molecular orbitals of the D, B and A fragments of 2a-Zn-CN (Fig. 5). The red lines represent the charge transfer integrals between these states. All computations were performed with the ADF program [44].

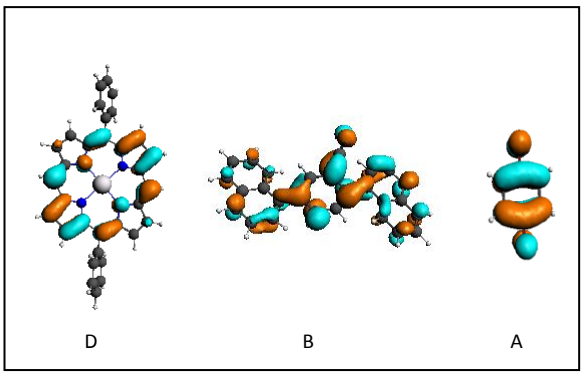


**Fig. 7** The LUMO orbitals of the isolated D, B and A fragments of the 2a-Zn-CN (Fig. 5). The B LUMO (middle) is delocalized over the phenyl ring and the connecting naphthalenes.

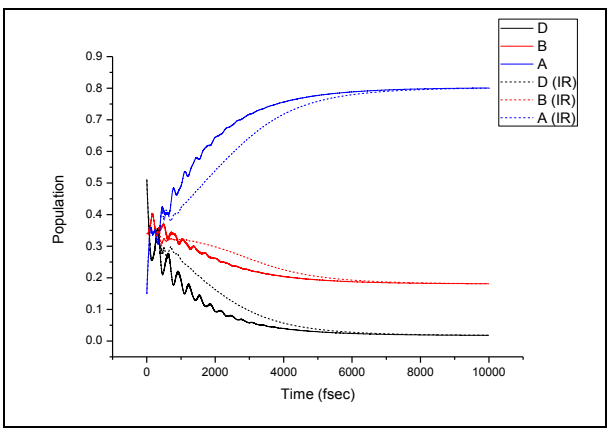


**Fig. 8** Time evolution of D, B and A probabilities with and without the IR pulse for the model in eqn (7-8) using some of the parameters computed for the 2a-Zn-CN molecule (Figs. 5-6). The electronic Hamiltonian parameters are: $E_D^0 = 0eV$, $E_B^0 = -0.24eV$, $E_A^0 = -0.57eV$ and $V_{DB}^{el} = 0.233eV$ $V_{AB}^{el} = 0.237eV$. $E_B^0$ is brought to a value between $E_D^0$ and $E_A^0$ while maintaining initial-to-final vibronic state resonance. The vibrational and electronic-vibrational Hamiltonian parameters are $\hbar\omega_B = 0.28eV$, $\hbar\omega_A = 0.2eV$, $a_B = 0.11eV$ and $a_A = 0.15eV$. The vibrational relaxation time scales are psec, $\hbar\Gamma_B^{rel} = \hbar\Gamma_A^{rel} = 0.0007eV$. For the IR-perturbation, $a_{IR} = 0.06eV$, $t_0 = 500f\,\sec$ and $\sigma_{IR} = 100f\,\sec$. The effect of IR-excitation is significant, giving $I_D \approx 0.35$ and $I_A \approx 0.1$ (eqn (14) with T= 6 psec). Observe that in this system $V_{DB}^{el} / \hbar\Gamma_B^{rel} \approx 333$ and $V_{AB}^{el} / \hbar\Gamma_B^{rel} \approx 338$. Defining the ET time scale $\tau_{ET}$ to be approximately the time when the unperturbed acceptor probability passes through ~50% ( $P_A \approx 0.5$), and $\tau_B^{rel} \approx 1/\Gamma_B^{rel}$, we have $\tau_B^{rel} \approx 1000f\,\sec$ and $\tau_{ET} \approx 1000f\,\sec$.

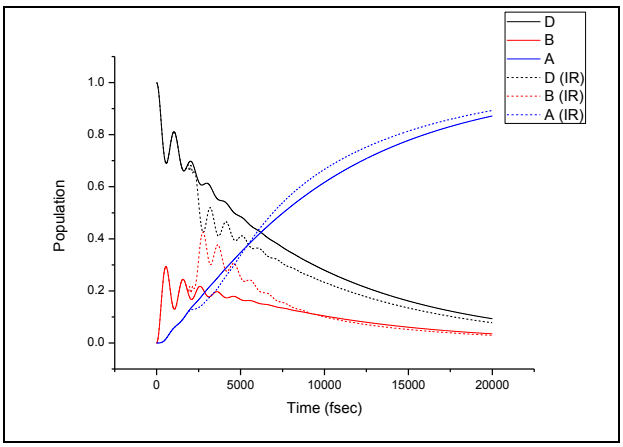


**Fig. 9** As in Fig. 8 but with weaker couplings ($V_{DB}^{el} = 0.003eV$, $V_{AB}^{el} = 0.002eV$), such that the ratios $V^{el} / \hbar\Gamma_B^{rel}$ are lowered ( $V_{DB}^{el} / \hbar\Gamma_B^{rel} \approx 4, V_{AB}^{el} / \hbar\Gamma_B^{rel} \approx 3$). The pulse is applied at $t_0 = 2000f\,\sec$, and the other parameters are the same as in Fig. 8. The effect of IR-excitation is not very different from Fig. 8 for the D fractional yield, $I_D \approx -0.13$, but it is reduced for the acceptor fractional yield, $I_A \approx 0.04$. For this system $\tau_B^{rel} \approx 1000f\,\sec$, and $\tau_{ET} \approx 7600f\,\sec$.

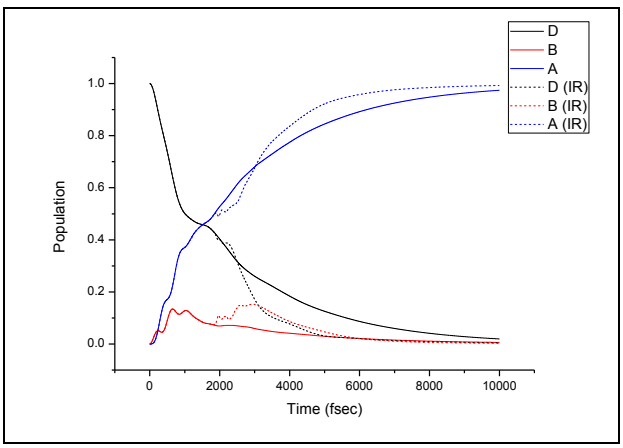


**Fig. 10** As in Fig. 9 but with very asymmetric inter-site coupling ( $V_{DB}^{el} = 0.003eV$, $V_{AB}^{el} = 0.02eV, V_{DB}^{el} / \hbar\Gamma_B^{rel} \approx 4, V_{AB}^{el} / \hbar\Gamma_B^{rel} \approx 30$). The pulse is applied at $t_0 = 2000f\,\sec$ and the other parameters are the same as in Fig. 9. The effect of IR-excitation is comparable to Fig. 9, with $I_D \approx -0.21$ and $I_A \approx 0.04$. For this system $\tau_B^{rel} \approx 1000f\,\sec$ and $\tau_{ET} \approx 1870f\,\sec$.

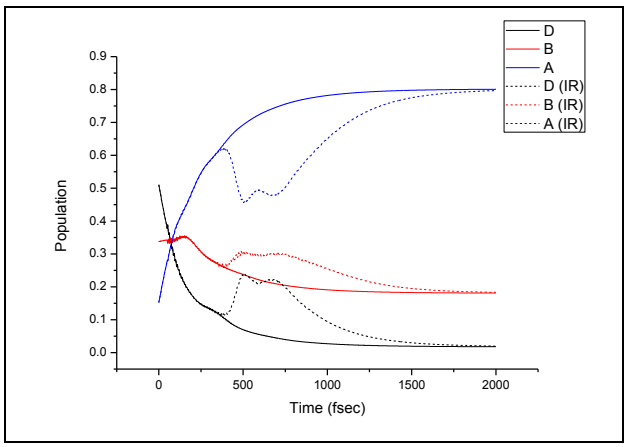


**Fig. 11** As in Fig. 8 but with faster vibrational relaxation time scales of 164 fsec ($\hbar\Gamma_B^{rel} = \hbar\Gamma_A^{rel} = 0.004eV$), giving $V_{DB}^{el}/\hbar\Gamma_B^{rel} \approx 60$ and $V_{AB}^{el}/\hbar\Gamma_B^{rel} \approx 60$. The pulse is applied at $t_0 = 500\,f\,\mathrm{sec}$ and the other parameters are the same as in Fig. 8 The effect of IR-excitation on the D yield is large, $I_D \approx 0.7$ ( $I_A \approx -0.1$). For this system $\tau_B^{rel} \approx 164\,f\,\mathrm{sec}$ and $\tau_{ET} \approx 207\,f\,\mathrm{sec}$.

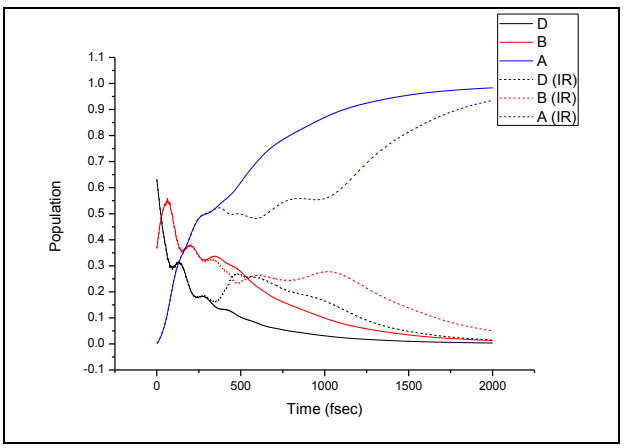


**Fig. 12** As in Fig. 11 (164 fsec vibrational relaxation) with asymmetry in the electronic couplings giving $V_{DB}^{el}/\hbar\Gamma_B^{rel} \approx 60$ and $V_{AB}^{el}/\hbar\Gamma_B^{rel} \approx 5$. The pulse is applied at $t_0 = 500\,f\,\mathrm{sec}$. For this system $\tau_B^{rel} \approx 164\,f\,\mathrm{sec}$ and $\tau_{ET} \approx 292\,f\,\mathrm{sec}$ and $I_D \approx 0.93$ and $I_A \approx -0.19$.

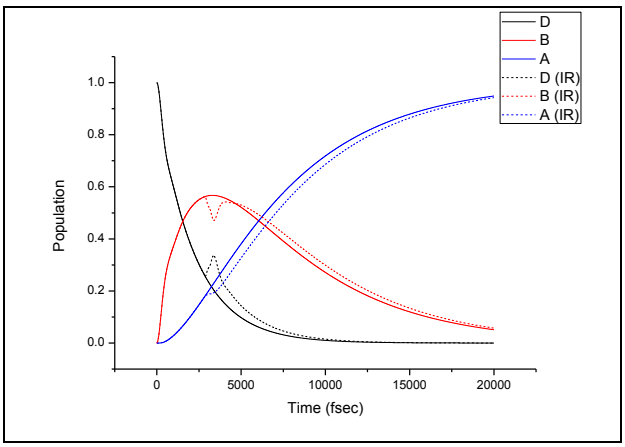


**Fig 13** As in Figs. 11 and 12 (vibrational relaxation time scales of 164 fsec), but with reduced couplings giving $V_{DB}^{el}/\hbar\Gamma_B^{rel} \approx 0.75$ and $V_{AB}^{el}/\hbar\Gamma_B^{rel} \approx 0.5$. The pulse is applied at $t_0 = 3000\,f\,\mathrm{sec}$, and the other parameters are the same as in Fig. 12. The effect of IR-excitation is greatly diminished, $I_D \approx 0.1$ and $I_A \approx -0.04$ because the ratios $V^{el}/\hbar\Gamma_B^{rel}$ are below unity. For this system $\tau_B^{rel} \approx 164\,f\,\mathrm{sec}$ and $\tau_{ET} \approx 6326\,f\,\mathrm{sec}$.

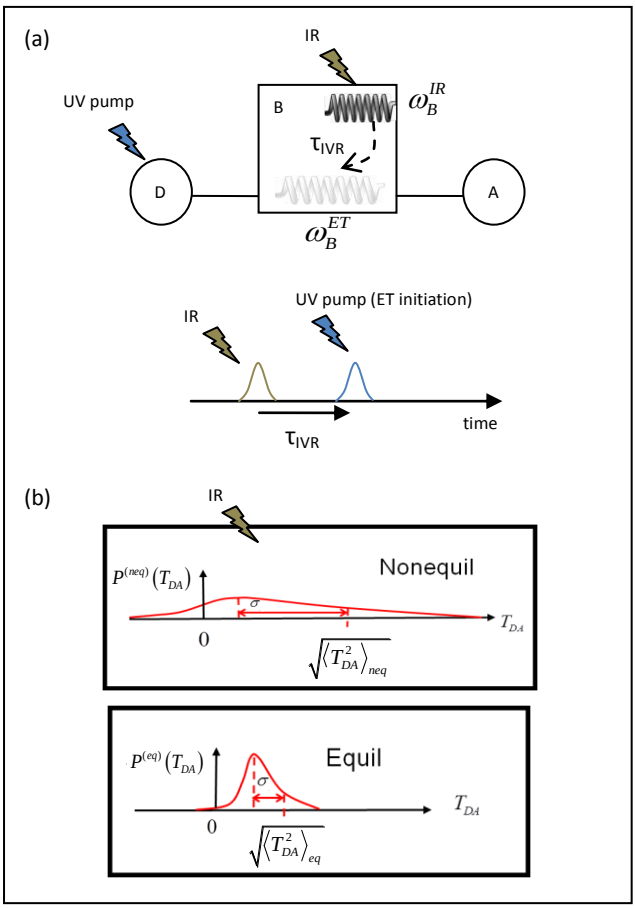


**Fig. 14**. The nonadiabatic ET time scales are much slower than vibrational energy redistribution time scales. Due to the long distance between D and A, low-frequency bridge modes modulate the bridge-mediated D-A tunneling matrix element. Low frequency modes cannot be selectively excited by IR and lose their excitation energy very fast to the continuum. In this situation a design principle for perturbing the ET rate with IR is to use high frequency IR active modes that dump their energy to the low-frequency ET-active

modes (a). If this energy transfer is of a time scale $\tau_{IVR}$, the IR excitation must be applied a time $\tau_{IVR}$ prior to the UV (VIS) excitation that initiates ET. This strategy will create a nonequilibrium bridge structural ensemble and a corresponding non-equilibrium $T_{DA}$ ensemble described by a probability density $P^{neq}\left(T_{DA}\right)$ (14b, upper). If $P^{neq}\left(T_{DA}\right)$ is sufficiently different from the thermal (equilibrium) probability density $P^{eq}\left(T_{DA}\right)$ (4b, lower), the nonadiabatic ET rate will change upon excitation with IR.

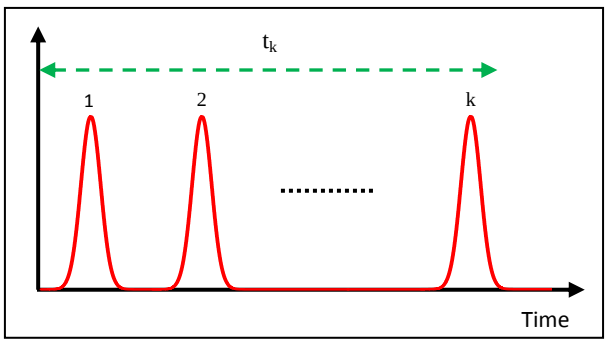


**Fig. A1:** Representation of the generated pulses. K:number of pulses in time interval $t_k$

| $t_0$ | $I_D$ | $I_A$ |
|---|---|---|
| 200fsec | -0.404 | 0.083 |
| 1000fsec | -0.343 | 0.078 |
| 2000fsec | -0.216 | 0.032 |
| 4000fsec | -0.080 | 0.008 |

**Table I (Fig. 10)** D and A fractional yields (eqn (14)) as a function of IR pulse delay $t_0$ for the system of Fig. 10 (vibrational relaxation time of psec, $V^{el}/\hbar\Gamma_B^{rel}>1$). The effect of the IR-pulse is larger for the D yield and it is maximized for the shorter time delays (35-40%).

| $t_0$ | $I_D$ | $I_A$ |
|---|---|---|
| 200fsec | 0.598 | -0.106 |
| 500fsec | 0.698 | -0.112 |
| 700fsec | 0.739 | -0.122 |
| 1000fsec | 0.751 | -0.126 |

**Table II (Fig. 11)** D and A fractional yields (eqn (14)) as a function of IR pulse delay $t_0$ for the system of Fig. 11 where the vibrational relaxation time is reduced to 164 fsec and $V^{el}/\hbar\Gamma_B^{rel}>1$. The effect of the IR-pulse is enhanced for the D yield compared to the case of Table I and it remains relatively constant as a function of the delay time. The yield perturbation is of the order of 70 % for D and 10% for A.

| $t_0$ | $I_D$ | $I_A$ |
|---|---|---|
| 200fsec | 0.954 | -0.171 |
| 300fsec | 0.818 | -0.150 |
| 500fsec | 0.931 | -0.189 |
| 700fsec | 0.963 | -0.216 |
| 1000fsec | 0.883 | -0.206 |

**Table III (Fig. 12)**

D and A fractional yields (eqn (14)) as a function of IR pulse delay $t_0$ for the system of Fig. 12 with unsymmetric electronic couplings and $V^{el}/\hbar\Gamma_B^{rel}>1$ (vibrational relaxation time of 164 fsec). The effects of the IR-pulse remain relatively constant as a function of the delay time. The yield perturbation is of the order of 100% for D and 20% for A.

| $t_0$ | $I_D$ | $I_A$ |
|---|---|---|
| 200fsec | -0.079 | 0.015 |
| 1000fsec | -0.012 | -0.037 |
| 3000fsec | 0.122 | -0.039 |
| 5000fsec | 0.139 | -0.038 |
| 6000fsec | 0.132 | -0.035 |

**Table IV (Fig. 13)** D and A fractional yields (eqn (14)) as a function of IR pulse delay $t_0$ for the system of Fig. 13 (vibrational relaxation time of 164 fsec). The effects of the IR-pulse on the yields are reduced compared to Table II and III because $V^{el}/\hbar\Gamma_B^{rel}<1$.